10th International Conference on Fracture Mechanics of Concrete and Concrete Structures
FraMCoS-X
G. Pijaudier-Cabot, P. Grassl and C. La Borderie (Eds)
https://doi.org/10.21012/FC10.232890

EXPERIMENTAL STUDY AND NUMERICAL MODELING ON BOND BETWEEN STEEL REINFORCEMENTS AND STRAIN-HARDENING CEMENTITIOUS COMPOSITES (SHCC)

YIXIN CHEN[*] AND CHRISTOPHER K. Y. LEUNG[*]

[*] The Hong Kong University of Science and Technology
Hong Kong, China
e-mail: ychenbu@connect.ust.hk, and ckleung@ust.hk

Key words: Bond-slip behavior, Strain-hardening cementitious composite (SHCC), Steel reinforcement, Finite element modeling

Abstract: Strain-hardening cementitious composites (SHCC) are a type of pseudo-ductile material characterized by its tensile strain-hardening behavior, high tensile ductility and crack control capability. In many structural applications of SHCC, especially in repair work and joining of precast elements, good bonding with steel reinforcements is required to guarantee the stress transfer. Thus, the bond property between steel rebars and SHCC is an important issue to investigate. This paper presents the experimental testing and numerical modeling of the bond between deformed steel rebars and high strength SHCC. Bond test in direct tension is performed on specimens made of rebars and SHCC or concrete cover. The effects of materials, cover thicknesses and rebar sizes on the bond behavior are discussed. For the numerical simulation, instead of using a detailed model that involves complex geometry and comprehensive bond mechanisms, a simplified finite element model is adopted, which integrates all non-linear behaviors into spring elements linking SHCC and steel rebar elements. The spring behavior is back-fitted according to the experimentally determined load-displacement relation. To verify the effectiveness of the model, the modeling and experimental results for different specimen configurations are compared. The study reveals that the bond property between steel rebars and SHCC is superior to that between steel rebars and normal concrete, and that the cover thickness has a great influence on the bond strength. Further, the simple numerical model provides an effective method to extract the bond stress-slip behavior so that it can be used to determine the bond length for more general cases.

1 INTRODUCTION

Developed in 1990s under the guidance of fracture mechanics and micromechanics [1], strain-hardening cementitious composites (SHCC) are a type of composites with strain-hardening behavior and tensile ductility, as well as the ability of crack control. Through many research studies and engineering applications, SHCC has been proved to be effective not only in the construction of infrastructures and buildings, but also in joining precast concrete elements [2] as well as structural repair [3]. Among these structural applications of SHCC, the bond length between steel rebar and SHCC is often a critical design parameter to be determined, as it will affect the stress transfer from steel to SHCC and thus may affect the performance of the whole structure. In the authors' previous study of a novel repair method for deteriorated reinforced concrete structures with corroded reinforcements, the repair effectiveness relied on the load carried by the SHCC, which is governed by the stress transfer from the steel rebar to SHCC through the bond [3].

Insufficient bond length would reduce the load capacity recovery of the structure. Therefore, it is important to investigate the behavior of the bond between steel reinforcements and SHCC.

Researchers have proposed different test method to investigate the bond between steel rebar and the covering concrete. In [4-6], the rebar was pulled at one end where the covering block was being pushed. While this test is easy to perform, the major drawbacks is that the compressive stress in the block does not reflect the actual stress state in many cases, and may increase the resistance to the cracking in the cover. Also, the transverse friction at the pushing interface will also restrain the splitting cracks., resulting in improved bonding. Another method takes into consideration the bending effect occurred in structures (e.g. beams) [7, 8], but it involves complicated test setup and measurement. While in [9, 10], the specimens adopted was a simple block with two rebars embedded in both sides and tested under direct tension. In this test method, good alignment of the two rebars has to be ensured.

Numerical modeling of the bond between rebar and concrete, fiber reinforced concrete or SHCC has also been a topic of interest in many studies. Due to the complexity of the problem especially when deformed rebars are involved, simplification techniques have to be adopted. For instance, in [11], the frictional and mechanical components of the bond were combined and considered by using specially designed bond elements. In [12], the bond between deformed rebar and concrete was simplified into a contact problem, but the study was only able to model the pre-peak behavior. In [7, 13], the geometry of the ribs was considered in the models but was simplified into a ring-shape profile. Such simplification is not very reasonable as the transverse area of the ribs should be distributed along the rebar, instead of concentrated in a certain section. Nevertheless, to construct a computationally feasible model, a compromise between efficiency and accuracy has to be reached.

In this study, pull-out bond test under direct tension is performed. Specimens are prepared with different deformed steel rebar sizes and different cover thicknesses of SHCC or plain concrete blocks. The pull-out load-slip relationships are compared and effects from different factors are discussed. Based on the experiment, a simplified numerical model consisting of linear elastic steel and SHCC materials as well as non-linear interface is constructed and analyzed using finite element modeling software ANSYS. The apparent bond stress-slip relationships were back-fitted according to the experimental results, as was done in [14, 15] for the bond between fiber reinforced polymer and concrete. The general applicability of the model was then verified through further experiments.

2 EXPERIMENTAL PROGRAM

2.1 Materials

The SHCC in this study was adopted from the authors' previous study in [3], with a composition shown in Table 1. This SHCC is characterized by high tensile strength of over 10 MPa and strain capacity more than 2% (Figure 1). To achieve such high strength, 20% of the cement was replaced by silica fume which has a much finer particle size and pozzolanic reactivity, making the microstructure of the material denser. Also, an ultra-low water-to-binder ratio of 0.145 was used, and super-plasticizer was added in a relatively high dosage to maintain proper workability. Sand content was limited to facilitate the dispersion of fibers. The fibers in the SHCC (2.2% in volume fraction) were polyethylene (PE) fibers, 12 mm in length and 24 μm in diameter. Table 1 also presents the mix composition of the plain concrete used in this study, with a target compressive strength (cylinder) of 50 MPa, similar to the commonly used high strength concrete C60. The steel reinforcements were all deformed rebars made of high yield steel, with yield strength of no less than 460 MPa.

2.2 Specimen Preparation and Testing Procedures

The experimental program was mainly to investigate different effects of brittle concrete and ductile SHCC on the overall bond behavior, as well as the effects of cover thickness and existence of lateral confinement.

Table 2 shows the specimen configurations and Figure 2 illustrates the specimen geometry. The letter in the beginning of the specimen ID represents the block material type, either concrete (C) or SHCC (S). The following two digits represent the diameter (in mm) of the rebar being pulled out, and the last two digits identify the cover thickness (in mm). The letter "C" at the end represents the existence of confinement. For each specimen, two major rebars with the same diameter were embedded in a block on each side of the specimen with different embedment lengths. The one with shorter embedment length (4*D*, *D* is the rebar diameter) was expected to fail in bond, while the longer-embedded one served as the anchorage end. The cover thickness to be studied was either *D* or 2*D*. Steel wire with 3.5 mm in diameter was used as the confinement for qualitative comparison although its size is not representative of actual applications. Four smaller minor rebars were placed through the whole specimen to prevent tensile failure of concrete or SHCC block at the gap between the two major rebars. Such minor rebars were placed at a distance from the major rebar in order to reduce their effect on the bond property of the major rebar. At least two specimens of each type were fabricated and tested.

Apart from the specimens in Table 2, smaller and larger scaled specimens (S1616, S2525) based on S2020 were prepared (Table 3). In addition, specimens similar to S2020 but with longer embedment lengths (5.5*D* for S2020-55, 7*D* for S2020-70) were also cast (Table 3).

Prior to casting, the minor rebars were fixed into position by the wooden mold, and the two major ones were installed using a stiff aligning fixture to ensure the alignment so as to minimize the bending effect. For SHCC specimens, cement, silica fume and sand were first dry mixed in a mortar mixer. Water as well as super-plasticizer were then added and mixed until it appeared flowable. PE fibers were subsequently added into the mortar and mixed until they were sufficiently well dispersed. The fresh mixture was cast into the mold with care to ensure the rebars were well covered. The specimens were demolded at 48 hours, after which they were cured at a temperature of 23 ± 2 ℃ and relative humidity of 95 ± 5 % until 14 days after casting, in accordance with the authors' relevant studies [3]. While for concrete specimens, similarly, dry materials were mixed first before water was added and mixed. Vibrating table was used for compacting. The specimens were demolded after 24 hours and cured in the above-mentioned condition until the age of 28 days.

Along with the pull-out specimens, three SHCC cylinders 50 mm in diameter and 100 mm in height and three concrete cylinders 100 mm in diameter and 200 mm in height were also prepared for acquiring their cylindrical compressive strength, elastic moduli and Poisson's ratios at the age of 14 days (SHCC) or 28 days (concrete).

The direct tensile pull-out tests were performed using a servo-hydraulic machine, as shown in Figure 3. The rebars at two ends were secured into the pressurized grips, and an initial displacement-controlled rate of 0.1 mm/min was adopted. Two linear variable displacement transducers (LVDT) were attached to the sides of the specimen for measuring the elongation of a region shown in Figure 2. When the load started to show a consistent decreasing trend, the rate was gradually increased to 1.5 mm/min, until a displacement of around 12 mm, which is approximately the spacing of the ribs on the deformed rebar.

2.3 Results and discussions

The material properties are summarized in Table 4, and the pull-out test results are shown in Table 5. Figure 4 (a) and (b) presents the average pull-out load-slip curves of different specimens (one specimen for each type) till the slip of 1 mm and 10 mm, respectively, while Figure 5 shows photos of different failure modes. The average bond stress in Table 5 was calculated directly through dividing the load by the cylindrical contact area between the block and the steel rebar. The pull-out slip in Figure 4 was interpreted from the LVDT readings.

According to the results shown in Figure 4, it is obvious that the bond behaviors of the specimens made of concrete and SHCC were distinct from each other in terms of both the bond strength and the shape of the curve. The ones made of SHCC showed much higher bond strength (Figure 4) followed by gradual decrease, while the concrete counterparts exhibited a sudden drop after the peak was achieved. Such sudden drop was related to the splitting of concrete cover during pull-out, and this wide splitting crack greatly reduced the contact between rebar and concrete, leading to a bond failure (Figure 5(a)). However, for SHCC specimens, due to the multiple-cracking characteristics, even if splitting cracks appeared, they were bridged by the PE fibers across them so the width was limited. The bond was weakened to some extent but the surrounding material remained as a whole to continue to bear against the ribs on the rebar. During the pushing of the ribs, the splitting force became larger and thus more and more splitting cracks occurred. After the peak load, some of the splitting cracks could not take up further load and thus widened (Figure 5(b)), or conical spalling took place at the pull-out surface about the same time (Figure 5(c)), and the bond stress started to descend. The failure was still in ductile manner (Figure 4), thanks to the softening tensile behavior of SHCC. When the rebar was pulled out completely, it could be observed that the ribs of the rebar carries some SHCC remains (Figure 5(d)), indicating that bearing failure was also involved in the overall bond failure. One may argue that it was the high strength of SHCC that contributed to the superior bond strength compared to concrete. It should be pointed out that the first splitting cracks of S2020 specimens appeared at the loading of only 25-30 kN. Were it not for the bridging of fibers, they would exhibit similar brittle failure like the concrete specimens at similar loads (around 25 kN for C2020), and even lower residual strength due to the lack of coarse aggregates.

The effect of cover thickness was straightforward. A larger cover thickness could reduce the tensile stress that caused splitting, and therefore delayed the failure to a higher load. The improvement in bond strength was significant with doubling the cover thickness for both concrete (43%) and SHCC (57%) specimens (Table 5), but the bond strength was less than doubled as the splitting tensile stress was not uniformly distributed through the cover. And more importantly, comparing SHCC specimens S2020 and S2040, the failure mode shifted from splitting failure to end spalling failure (Figure 5(e)), so the cover splitting did not govern the peak load.

Regarding the confinement, it was effective for the bond strength of the C2040C specimens, demonstrating 9% stronger bond than C2040 (Table 5). After the sudden drop caused by concrete splitting, the confining wire prevented the crack from sudden wide opening, so that the surrounding of the rebar was secured and could take further load, so the residual bond stress was also higher. The failure mode changed from splitting to spalling (Figure 5(f)). On the other hand, for S2040C specimens, the confinement was not as effective (only provided 0.5% improvement, Table 5), which was because the well-controlled splitting crack (due to PE fiber bridging) did not provide enough deformation for the wire to take effect.

Overall, it is clear that the ductility of covering material and a thicker cover can have a significant enhancement on the bond with steel rebars. The confinement only helps improve the bond when the covering material is brittle.

3 NUMERICAL MODELING

In applications where the stress transfer between SHCC and steel rebar is an important aspect, the condition of the bond usually varies as the rebar sizes, cover thickness and mechanical properties of the SHCC may be different. Thus, it is not practical to determine the required bond length through conducting numerous bond tests for each case. Instead, using numerical models based on a few experimental results for design purpose would be a reasonable solution. In numerical modeling, the balance between efficiency and accuracy should be determined in a way to best serve the purpose of modeling. There have been a great number of attempts to model the bond between steel rebar and its covering material, which can take into consideration many factors including frictional bond [11], mechanical interlocking [7, 11, 13], constitutive property and even inhomogeneity of the covering material [7, 13], etc. However, as more details are added to the model, more input data is needed which is mostly determined through experiment (e.g. the mechanical property of the covering materials). The errors coming from various input sources will then add up, making the model neither accurate nor efficient. In this study, an efficient model integrating all non-linear behaviors (chemical and frictional bonds, mechanical interlocking, splitting and spalling of SHCC) into one interfacial property was constructed. Such integration is based on the consideration that the SHCC block remained as a whole throughout the pull-out process, so that the stress distribution in SHCC and on the interface did not change substantially. For concrete blocks, however, after the splitting crack occurred, the stress field near the crack was totally different from the state before cracking. Thus, the numerical model was only applied for the SHCC specimens. The integrated interfacial property, or the apparent bond stress-slip relationship was first back-fitted using experimental results, and the effectiveness of the model was verified through additional bond tests described in the previous section.

The finite element modeling software ANSYS was used in this study. Element types three-dimensional SOLID185, two-dimensional LINK180 and the multi-linear spring COMBIN39 were used to model SHCC, steel rebar and their interface, respectively. As mentioned, all sources of non-linear behaviors were included in the spring elements, so the SHCC and rebar elements can hence be considered linear elastic. To further improve the modeling efficiency, only a quarter of the embedment region of the specimen was modeled (Figure 6(a)). Additionally, assuming the axial tensile stress of the rebar to be uniform across any transverse section (ignoring shear lag effect in the radial direction), instead of using three-dimensional elements to model the complete major rebar, its area was distributed at the interface, with a coupled series of two-dimensional link elements representing the distributed area on the interface (Figure 6(a)). The coincident nodes of rebar and SHCC elements were linked by the non-linear spring element, so that the relative displacement (slip) was the elongation of the spring (Figure 6(b)). Material properties of SHCC were adopted from Table 4. As for steel, the elastic modulus and Poisson's ratio were assumed to be 200 GPa and 0.3, respectively. The first step of the modeling was to back-fit the parameters of the multi-linear springs with the test results. Figure 7 shows the back-fitted results of bond behavior (until a relative displacement of 2 mm) for S2020 and S2040, and their corresponding load-slip curves. It is obvious that the bond stress-relative movement curves resemble the pull-out load-slip curves, implying that the bond stress and the slip can be regarded uniform along the rebar, which is reasonable since the axial stiffness of the steel results in negligible axial elongation compared to the slip.

Through such analysis the apparent bond stress-slip relationship of the bond configuration in S2020 can be extracted. To verify the feasibility of this relationship, it was input into the models of specimens with different configurations. Two proportionally scaled types of specimens (S1616 and S2525), and two other types with different bond lengths (S2020-55 and S2020-70) were tested for verification purpose, all of which had the cover equal to the rebar diameter. The results of modeling and testing are compared in Figure 8. For the scaled specimens, the numerical results could well match the experimental data (Figure 8(a)), with deviations within about 10%. Such deviation may be attributed to the size effect related to the unproportional scaling of rebar profiles. As shown in Table 6, although the height of the ribs on the rebar was 15% of the measured diameter for all of Y16, Y20 and Y25 rebars, the spacing of the ribs did not follow the scaling ratio but maintain similar absolute values. This could affect the mechanical interlocking mechanism—as the rebar size increased, the bearing area (related to rib height) was larger but the shear plane (related to rib spacing) remained similar, and thus the interlocking mechanism was different for scaled specimens. This statement is consistent with the curves in Figure 8(a) (the modeling yielded a higher curve for S2525 and a lower curve for S1616). Nevertheless, to address the size effect of the rebar, the model can be extended in the future by incorporating certain parameters characterizing the rebar profile based on sufficient investigation on the bond performance of different rebars.

In addition to scaling the size, changing the embedment length provides another aspect to verify the model. Figure 8(b) shows perfect replication for S2020-55 specimens with 5.5*D* bond length. For S2020-70, the model predicted a slightly lower peak load, but the residual stress after peak load matched well with the test data. This result also indicated that the bond stress was approximately uniformly distributed along the rebar, otherwise a longer embedment length would be less effective in improving the pull-out load.

According to the above discussions, the efficient and effective bond model proposed in this work is applicable to ductile covering materials. Although this method requires preliminary test for each type of geometry for back-fitting, or calibration of the apparent bond stress-slip relationship, the numerical output is very reliable. This modeling technique can also be extended to more complicated conditions, for example, the bond behavior under cyclic conditions, as long as the overall bond behavior obtained from the test can be input as the non-linear spring property.

4 CONCLUSIONS

This study presents the experimental investigation of the bond between steel and SHCC or concrete of different geometrical configurations. Finite element modeling of the bond behavior using the integrated bond stress-slip behavior is investigated, and its applicability has been verified. Based on the discussions, the following conclusions can be drawn:

(1) With the same geometry, SHCC can bond much better with steel rebars than ordinary concrete due to the well controlled splitting cracks. The cover thickness can improve the bond to some extent, while lateral confinement is only effective for brittle cover material.

(2) The numerical model integrating all bond mechanisms and non-linear effects into one set of interface parameters is effective and efficient for ductile covering materials as long as experimental data can be provided for back-fitting the apparent bond stress-slip relationship. It can then be used to calculate the pull-out behavior under more general cases, as well as determining the required bond lengths in structural design.

REFERENCES

[1] Li VC. From Micromechanics to Structural Engineering-The Design of Cementitious Composites for Civil Engineering Applications. J.Struct.Mech.Earthquake Eng., JSCE 1993;10(2):37-48.

[2] Choi H, Choi Y, Choi C. Development and testing of precast concrete beam-to-column connections. Eng Struct 2013;56:1820-1835.

[3] Chen Y, Yu J, Leung CK. Use of high strength Strain-Hardening Cementitious Composites for flexural repair of concrete structures with significant steel corrosion. Constr Build Mater 2018;167:325-337.

[4] Chu SH, Kwan A, Ng PL. Redesigning the test method for assessing the bond behaviour of reinforcing bar in concrete

2018.

[5] Xu S, Wang H. Experimental study on bond slip between ultra high toughness cementitious composites and steel bar. Engineering Mechanics 2008;11:53-61.

[6] Xiao J, Falkner H. Bond behaviour between recycled aggregate concrete and steel rebars. Constr Build Mater 2007;21(2):395-401.

[7] Bandelt MJ, Frank TE, Lepech MD, Billington SL. Bond behavior and interface modeling of reinforced high-performance fiber-reinforced cementitious composites. Cement and Concrete Composites 2017;83:188-201.

[8] Harajli M, Hamad B, Karam K. Bond-slip response of reinforcing bars embedded in plain and fiber concrete. J Mater Civ Eng 2002;14(6):503-511.

[9] Jin Q, Leung CK, Yu C. Effective joining method for pseudo-ductile permanent formwork. Mater Struct 2013;46(3):345-360.

[10] Cheung AK, Leung CK. Effective joining of pre-cast concrete slabs with self-compacting HSFRCC. Journal of Advanced Concrete Technology 2011;9(1):41-49.

[11] Lowes LN, Moehle JP, Govindjee S. Concrete-steel bond model for use in finite element modeling of reinforced concrete structures. Structural Journal 2004;101(4):501-511.

[12] De Nardin S, Almeida Filho FM, Oliveira Filho J, Haach VG, El Debs A. Non-linear analysis of the bond strength behavior on the steel-concrete interface by numerical models and pull-out tests 2005:1-12.

[13] Shafaie J, Hosseini A, Marefat MS. 3D finite element modeling of bond-slip between rebar and concrete in pullout test 2009:403-413.

[14] Leung CK, Klenke M, Tung WK, Luk HC. Determination of nonlinear softening behavior at FRP composite/concrete interface. J Eng Mech 2006;132(5):498-508.

[15] Pan J, Leung CK. Effect of concrete composition on interfacial parameters governing FRP debonding from the concrete substrate. Adv Struct Eng 2009;12(5):627-637.

Table 1: Mix composition of SHCC and plain concrete

	SHCC	Concrete
Cement	0.8	1
Silica fume	0.2	-
Sand	0.3	1.3
Aggregate	-	2
Water	0.145	0.45
Super-plasticizer	0.025	-
Fiber (vol.%)	2.2	-

Table 2: Specimen configuration

ID	Block material	Cover (mm)	Confinement
C2020	Concrete	20	No
C2040	Concrete	40	No
C2040C	Concrete	40	Yes
S2020	SHCC	20	No
S2040	SHCC	40	No
S2040C	SHCC	40	Yes

Table 3: Specimen configuration (for model verification)

ID	Rebar diameter *D* (mm)	Cover (mm)	Embedment length (mm)
S1616	16	16	64 (4*D*)
S2525	25	25	100 (4*D*)
S2020-55	20	20	110 (5.5*D*)
S2020-70	20	20	140 (7*D*)

Table 4: Summary of material test results for SHCC and concrete

	SHCC (14d)	Concrete (28d)
Compressive strength	108 MPa	49.9 MPa
Elastic modulus	41.2 GPa	30.3 GPa
Poisson's ratio	0.185	0.206

Table 5: Summary of pull-out test results

ID	Peak load (kN)	Average bond strength (MPa)	Failure mode
C2020	24.4	4.86	Splitting
C2040	34.8	6.93	Splitting
C2040C	37.9	7.54	Spalling
S2020	45.8	9.12	Splitting
S2040	71.9	14.3	Spalling
S2040C	72.3	14.4	Spalling

Table 6: Rib geometry (unit: mm)

ID	Inner diameter	Rib height*	Rib spacing^
S1616	15.3	2.35 (15%)	11.9 (5.0)
S2020	19.7	2.95 (15%)	12.2 (4.1)
S2525	24.2	3.65 (15%)	12.2 (3.3)

Note:
* Numbers in brackets refer to the ratio relative to the corresponding inner diameter.
^ Numbers in brackets refer to the ratio relative to the corresponding rib height.

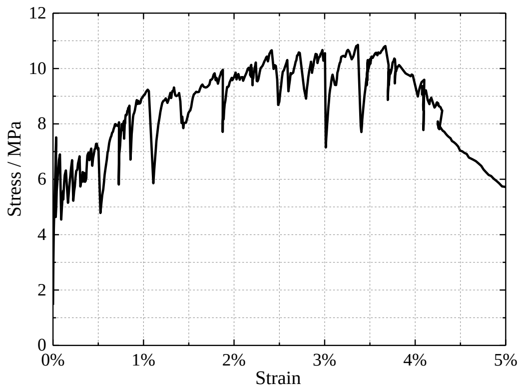

Figure 1: Typical tensile stress-strain curve for the high strength SHCC.

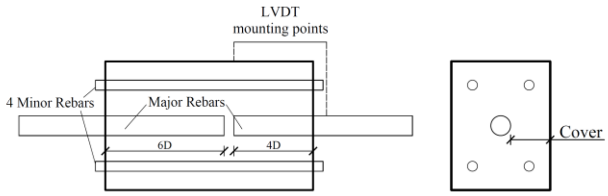

Figure 2: Specimen geometry.

Figure 3: Test setup.

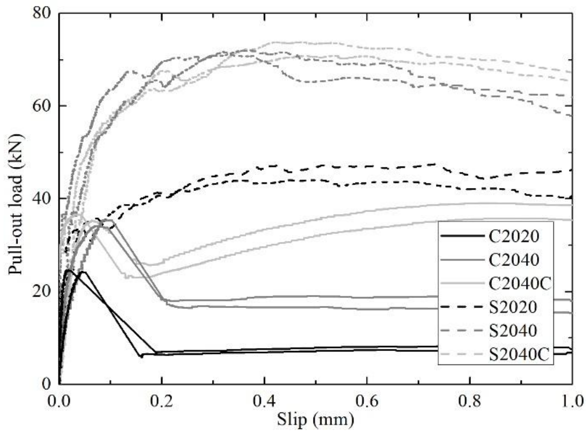

(a)

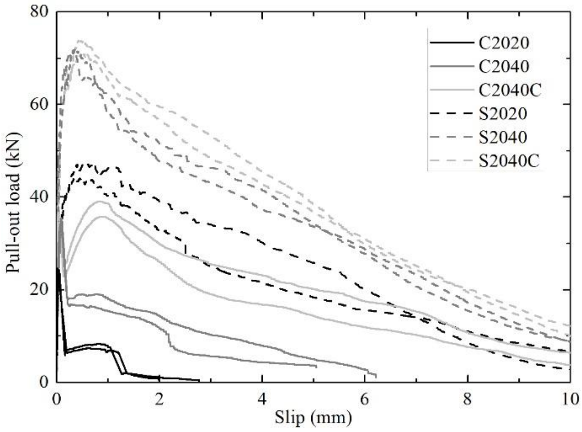

(b)

Figure 4: Pull-out load vs. slip curves.

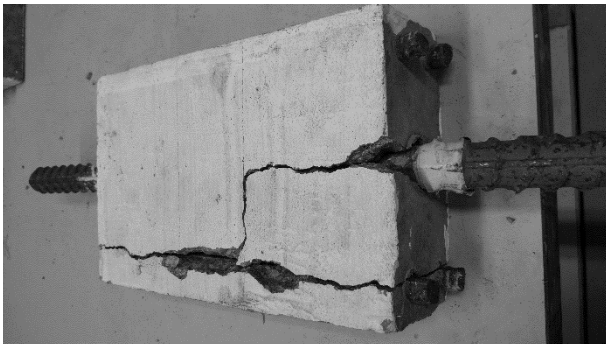

(a)

(b)

(c)

(d)

(e)

(f)

Figure 5: Failure modes.

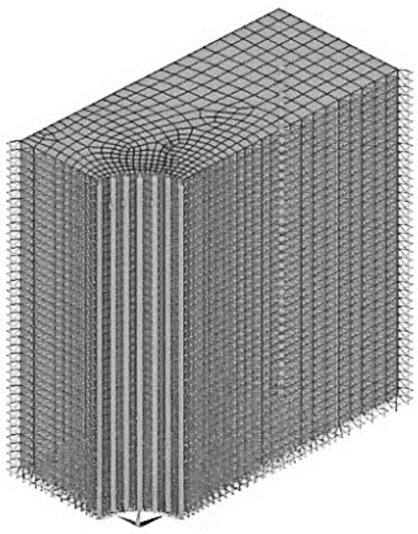

(a)

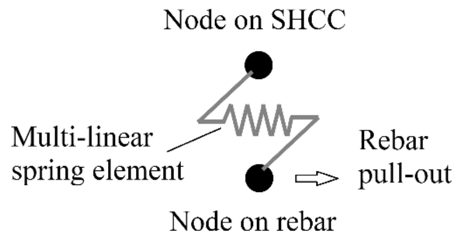

(b)

Figure 6: Finite element model of pull-out specimens.

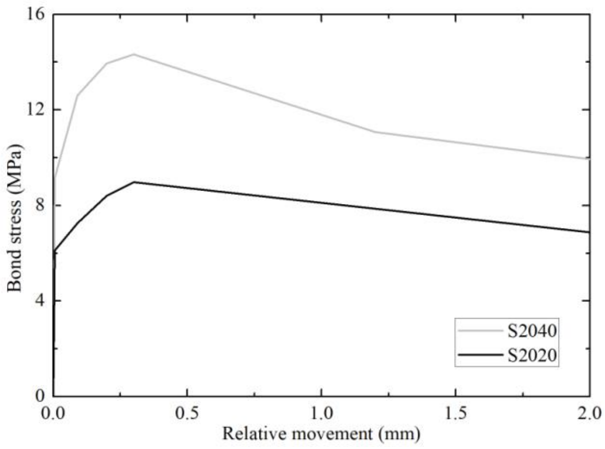

(a)

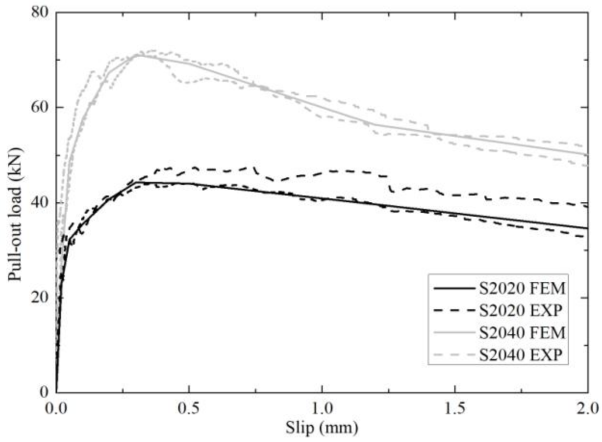

(b)

Figure 7: Back-fitting results for S2020 and S2040.

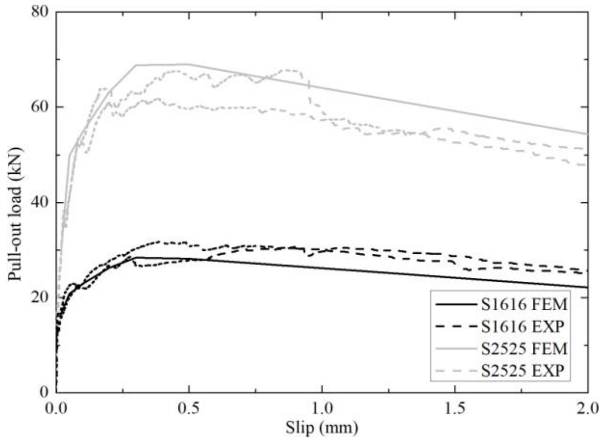

(a)

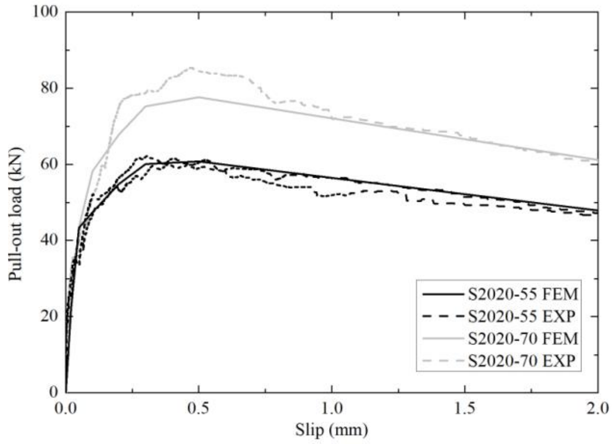

(b)

Figure 8: Comparisons between FEM and experimental results.